

Membrane Exporters of Fluoride Ion

Benjamin C. McIlwain,¹ Michal T. Ruprecht,¹
and Randy B. Stockbridge^{1,2}

¹Department of Molecular, Cellular, and Developmental Biology, University of Michigan, Ann Arbor, Michigan 48109, USA; email: stockbr@umich.edu

²Program in Biophysics, University of Michigan, Ann Arbor, Michigan 48109, USA

**ANNUAL
REVIEWS CONNECT**

www.annualreviews.org

- Download figures
- Navigate cited references
- Keyword search
- Explore related articles
- Share via email or social media

Annu. Rev. Biochem. 2021. 90:559–79

First published as a Review in Advance on
January 25, 2021

The *Annual Review of Biochemistry* is online at
biochem.annualreviews.org

<https://doi.org/10.1146/annurev-biochem-071520-112507>

Copyright © 2021 by Annual Reviews.
All rights reserved

Keywords

fluoride, Fluc, FEX, CLC, ion channel, antiporter, membrane protein

Abstract

Microorganisms contend with numerous and unusual chemical threats and have evolved a catalog of resistance mechanisms in response. One particularly ancient, pernicious threat is posed by fluoride ion (F^-), a common xenobiotic in natural environments that causes broad-spectrum harm to metabolic pathways. This review focuses on advances in the last ten years toward understanding the microbial response to cytoplasmic accumulation of F^- , with a special emphasis on the structure and mechanisms of the proteins that microbes use to export fluoride: the CLC^F family of F^-/H^+ antiporters and the Fluc/FEX family of F^- channels.

Contents

INTRODUCTION	560
FLUORIDE IN THE BIOSPHERE	560
Environmental Fluoride and Weak Acid Accumulation	560
Fluoride Ion Inhibition of Biomolecules	561
Biological Response to Fluoride Ion Toxicity	562
CHALLENGES IN FLUORIDE RECOGNITION	562
CLC ^F F ⁻ /H ⁺ ANTIPORTERS	564
CLC ^F Structure and Fluoride Coordination	565
CLC ^F Fluoride Transport Mechanism and Selectivity	567
FLUC F ⁻ CHANNELS	568
Architecture of Fluoride Channels	569
Fluc Fluoride Coordination and Proposed Permeation Pathway	571
The Unresolved Question of Fluoride Selectivity by the Flucs	573
CONCLUSIONS	573

INTRODUCTION

Nearly all microorganisms possess membrane proteins dedicated to the export of fluoride ion (F⁻). These proteins belong to one of two families, each of which has a completely different fold and exports F⁻ via a fundamentally different mechanism. The first group is a fluoride-specialized variant of the well-known CLC (Cl⁻ channel) family of anion transporters and channels called the CLC^Fs (CLC-fluorides). These proteins are secondary active transporters that harness the proton motive force to export F⁻ in exchange for proton (H⁺) import (1). The second family, called Fluc (fluoride channel) in bacteria and FEX (fluoride exporter) in eukaryotes, consists of dedicated fluoride channels that permit electrodiffusive export of F⁻ (2, 3). In the extensive catalog of ion channels and transporters, these were the first fluoride-handling proteins to be identified. Moreover, they draw a stark contrast with most cases of fluoride complexation by biological macromolecules in that they bind F⁻ without the aid of any metal ion.

Why are the CLC^Fs and Flucs so broadly distributed among microbes, and how do they work? This review first addresses the biological rationale for fluoride export, including where microbes encounter fluoride, why intracellular fluoride accumulation is harmful, and the mechanisms that microbes have evolved to mitigate this threat. We then discuss the physicochemical features that distinguish fluoride from other common biological anions and the molecular mechanisms by which the CLC^F and Fluc/FEX proteins exploit these differences to accomplish selective fluoride binding and export.

FLUORIDE IN THE BIOSPHERE

Environmental Fluoride and Weak Acid Accumulation

F⁻ has been abundant in the environment over evolutionary time (**Figure 1a**). Approximately 85 million tons of fluoride are concentrated in the Earth's mantle, and volcanic eruptions disperse hydrofluoric acid (HF) and H₂SiF₄ volatiles that can settle in soil or water. This halide is commonly found in groundwater, where leaching of rocks containing fluoride-rich minerals, such as fluorite, apatite, and muscovite, deposits F⁻ into aquifers. Clay soils are also abundant in F⁻, where the ion is often found in complex with cations like aluminum (Al³⁺) (4, 5). Natural environmental

Proton motive force:
the electrochemical proton gradient across the inner membrane established by the electron transport chain

Electrodiffusive:
passive flow of an ion down its electrochemical gradient

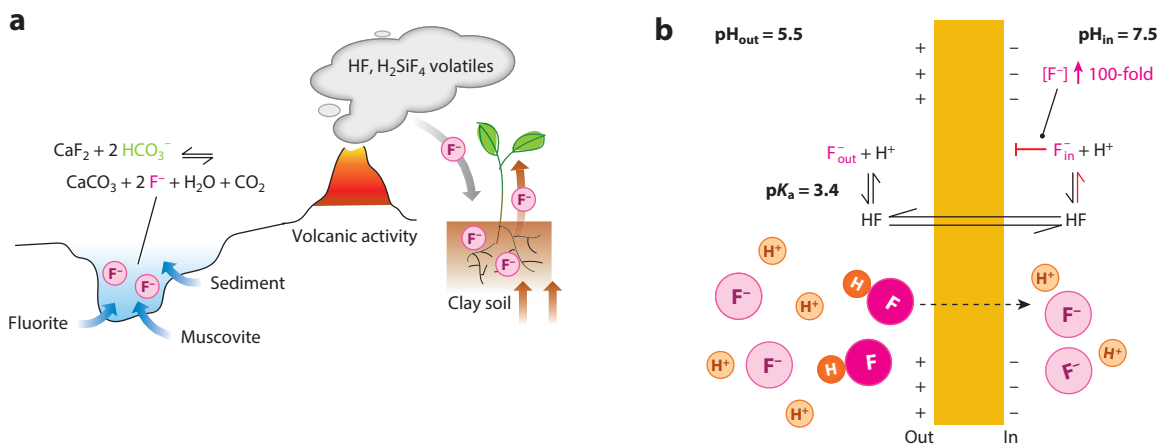


Figure 1

Environmental sources of aqueous and terrestrial fluoride and weak acid accumulation. (a) Alkaline environments rich in bicarbonate ion (HCO_3^-) promote exchange of F^- trapped in aquifer rocks. Volatile fluoride complexes are dispersed from deep within the Earth's crust via volcanic activity to the terrestrial surface, where they encounter plants and microbes. (b) Weak acid accumulation (ion-trapping) pathway for the intracellular accumulation of F^- in modestly acidic environmental niches. A two-unit pH differential across the membrane leads to a 100-fold elevation in intracellular fluoride over environmental levels according to Equation 1.

fluoride concentrations vary widely depending on the local geology and range from 30 to 80 μM in oceans and from 10 to 400 μM in ground and surface waters (4, 6). In some areas, human activity further increases ambient F^- concentrations over environmental levels. Fluoridation of municipal water supplies in the United States sets the F^- concentration of drinking water to $\sim 40 \mu\text{M}$ in many locations (7, 8), and F^- concentrations are higher still in areas affected by industrial pollution or use of fluoride-contaminated fertilizers and in niches such as the oral microbiome, where exposure to fluoride for dental hygiene—the concentration of F^- is $\sim 70 \text{ mM}$ in toothpaste—is routine (4, 9).

Thus, broadly dispersed microbes frequently encounter fluoride in their environment. Exposure to this halide is further exacerbated in acidic niches (**Figure 1b**). The conjugate acid HF is a weak acid ($\text{p}K_a = 3.4$), and because HF is small and uncharged, it readily crosses the plasma membrane (10, 11). Since microbes maintain their cytoplasm at a constant pH between 7 and 7.5, even during mild acid stress (12, 13), HF that crosses the plasma membrane encounters a relatively higher cytoplasmic pH, which shifts the equilibrium toward dissociation to a proton and F^- . These charged species cannot diffuse back across the membrane out of the cell and thus accumulate, a process known as weak acid accumulation or ion trapping (14). In microbes that lack any F^- export pathway, intracellular F^- accumulates according to this simple scheme:

$$\frac{[\text{F}^-]_{\text{in}}}{[\text{F}^-]_{\text{out}}} = \frac{[\text{H}^+]_{\text{out}}}{[\text{H}^+]_{\text{in}}} \quad 1.$$

For a microbe in a modestly acidic niche of pH 5.5 that maintains a cytoplasmic pH of 7.5, the intracellular fluoride accumulates 100-fold in the cytoplasm compared to environmental levels, reaching millimolar concentrations (15).

Fluoride Ion Inhibition of Biomolecules

Once it has breached the membrane and accumulated within the cell, fluoride is detrimental to biological systems because of its ability to act as substrate or transition-state analog for a host of metalloenzymes involved in the most fundamental biological processes, ranging from glycolysis to

Riboswitch:

a regulatory RNA element that alters gene transcription or translation in response to ligand binding

Membrane potential:

the difference in electrical potential across the membrane; a metabolizing bacterium typically has a negative-inside membrane potential of ~100 mV

nitrogen fixation to macromolecule synthesis (14, 16, 17). One common theme of enzyme inhibition by F^- is that the electronegative F^- effectively outcompetes electronegative substrate groups, such as OH^- , phosphate, and carboxylate, for coordination by an enzyme-bound metal ion. For example, in pyrophosphatase, F^- displaces the hydrolytic water in the coordination sphere of the enzyme-bound Mg^{2+} , acting as a transition-state analog of the activated water molecule (18, 19) (**Figure 2a**). In enolase, the enzyme that catalyzes the conversion of 2-phosphoglycerate to phosphoenolpyruvate during glycolysis, fluoride complexes an active-site Mg^{2+} , displacing the substrate's carboxylate group (20–23) (**Figure 2b**). Enzymes that catalyze phosphoryl group transfer reactions, including kinases and other ATP-consuming enzymes, are also subject to inhibition by fluoride-metal ion complexes like the trigonal planar aluminum trifluoride (AlF_3) adduct, which behaves as a transition-state analog for phosphoryl group transfer reactions, or beryllium trifluoride (BeF_3^-), which mimics the geometry of a phosphate and forms a ground-state analog together with ADP (24, 25) (**Figure 2c**). Since aluminum is also found at physiologically relevant concentrations in soils, aluminum fluoride inhibition of phosphoryl group transfer enzymes is a germane biological phenomenon (4). In these various examples, the inhibitory constants of F^- are in the hundreds of micromolar range, well within the range of cytoplasmic F^- accumulation that occurs in modestly acidic environmental niches (15).

Biological Response to Fluoride Ion Toxicity

Given the broad-spectrum sensitivity of metabolic processes to inhibition by fluoride, it is perhaps unsurprising that microbes possess mechanisms to mitigate this threat. However, the existence of the microbial fluoride response was unknown until 2012, when Ronald Breaker and colleagues (26) showed that the conserved *crcB* riboswitch motif (**Figure 2d**), present in all domains of life, acts as a transcriptional on switch upon F^- binding (see the sidebar titled The Fluoride Riboswitch). Genes commonly associated with bacterial fluoride riboswitches (**Figure 2e**) include fluoride-sensitive metalloenzymes like enolase and the ATP-consuming DNA repair enzyme MutS, shown in **Figure 2c**. Sodium ion (Na^+)/ H^+ antiporter genes also frequently cooccur with fluoride riboswitches. Because they help maintain pH homeostasis, the Na^+/H^+ antiporters may alleviate proton accumulation that occurs when HF enters the cell and dissociates. But the most frequently encountered genes, present in nearly half of all fluoride riboswitch-controlled operons, encode membrane proteins that have since been identified as F^- exporters, the CLC^F and Fluc proteins (**Figure 2f**).

By providing a route for accumulating F^- to exit the cell, expression of these F^- export proteins in the plasma membrane undermines weak acid accumulation of fluoride (1, 15, 26, 27). An extra thermodynamic push is provided by the proton motive force that metabolizing cells maintain. The CLC^F s harness the proton gradient directly by coupling fluoride export to proton import (1). For the Flucs, the positive-outside electrical potential thermodynamically favors anion expulsion (2). Although CLC^F and Fluc are unrelated by sequence, structure, and mechanism, their physiological roles overlap, and most bacteria have one or the other but not both. Fluoride exporters from the CLC^F and Fluc families are not necessarily associated with a riboswitch (1, 26); some, including the *Escherichia coli* Fluc channel, are instead constitutively expressed (15).

CHALLENGES IN FLUORIDE RECOGNITION

The common challenge shared—and met—by the CLC^F s and the Flucs is not only to rapidly export F^- but to do so with high specificity. Other anions like chloride (Cl^-) are more abundant in the cytoplasm [10–100 mM in *E. coli* (28)], and even low levels of uncontrolled leakage would disrupt the membrane potential with catastrophic consequences for processes that rely on the electrical potential, including ATP synthesis, secondary active transport, and motility.

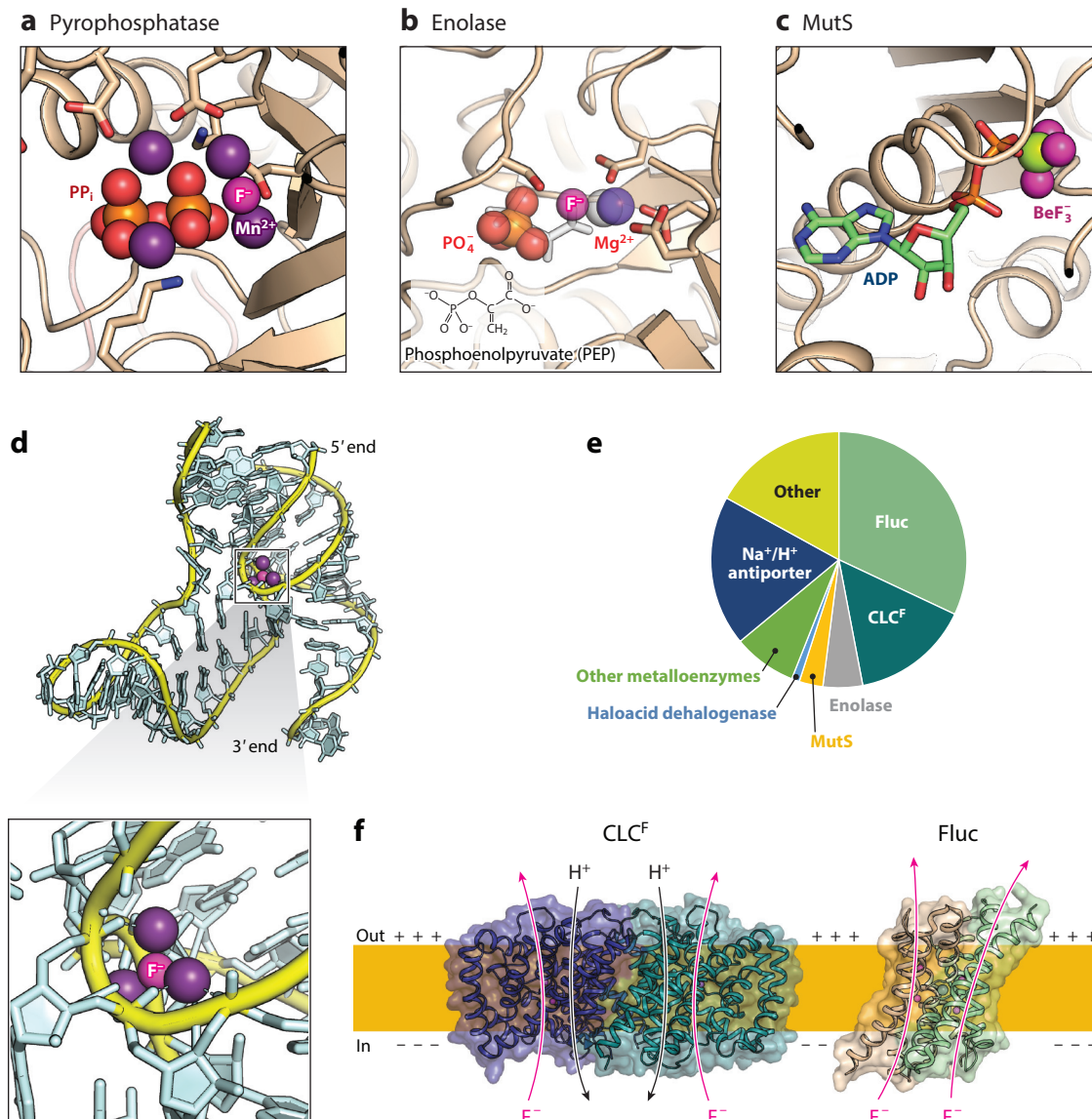


Figure 2

Biological responses to cytoplasmic fluoride accumulation. (*a–c*) Inhibition of enzymes by fluoride. F^- is shown as a pink sphere in each view. (*a*) Pyrophosphatase (PDB ID 1E6A). Pyrophosphate (PP_i) is depicted by orange and red spheres and Mn^{2+} by violet spheres. (*b*) Enolase (PDB ID 1NEL). The position of the natural product, phosphoenolpyruvate (*transparent white sticks*) complexed with Mg^{2+} (*white sphere*), is overlaid with the structure of the inhibitory $F^-/PO_4^-/Mn^{2+}$ complex (*red and orange spheres* represent PO_4^- , and *violet spheres* represent Mn^{2+}). F^- binds in the same position as the carboxylate group of the substrate or product. (*c*) The ATP-dependent DNA repair enzyme MutS (PDB ID 1NNE) with bound ADP (*sticks*) and BeF_3^- adduct (beryllium in *light green* and F^- in *pink*). Here, the BeF_3^- adduct mimics the terminal phosphoryl group of ATP. (*d, top*) Structure of the fluoride-sensing riboswitch of *Thermotoga petrophila* (PDB ID 4ENB). The F^- is shown as a pink sphere, and magnesium ions are shown in purple. (*d, bottom*) Zoomed-in view of the fluoride binding site. (*e*) Genetic association of fluoride-sensitive enzymes and fluoride exporters with fluoride riboswitches. Sections are proportional to the number of bacterial operons that encode each protein. (*f*) Riboswitch-associated fluoride exporters CLC^F and Fluc (PDB IDs 6D0J and 5NKQ, respectively). The membrane is indicated by the orange rectangle, with the typical membrane polarization indicated by plus and minus symbols. The direction of ion movement is shown for each protein. Abbreviations: PDB ID, Protein Data Bank identifier; PP_i , pyrophosphate. Pie graph in panel *e* adapted with permission from Reference 26.

THE FLUORIDE RIBOSWITCH

The discovery of fluoride as the ligand for this riboswitch family by the Breaker lab was unexpected and serendipitous (26, 99). While searching for the natural ligand for this conserved RNA motif, researchers observed activation upon the addition of various nucleotide substrates. But it was not nucleotide binding that threw the switch—the culprit turned out to be F^- , which was present at trace amounts from chemical synthesis (26). The apparent incongruence of a negative ion binding to a negatively charged RNA molecule has been resolved by structural studies (100, 101). Water molecules and five inward-pointing backbone phosphoryl groups coordinate three Mg^{2+} ions, which screen the negative charge. These Mg^{2+} ions, in turn, coordinate a single F^- ion. The structure of the fluoride- Mg^{2+} nucleus is reminiscent of the fluoride-inhibited pyrophosphatase structure (18), with RNA phosphoryl groups in place of the substrate pyrophosphate.

However, specificity cannot be achieved by tight binding, since ionic throughput is a critical functional feature of transport proteins. And, in contrast to the majority of F^- binding macromolecules, including those shown in **Figure 2a–d**, neither membrane exporter employs metal ions to bind or transport F^- , providing rare examples of biological F^- coordination without intervening metals.

Among the halides, F^- and Cl^- are the most similar, and discriminating these anions has proved to be quite difficult in synthetic applications, particularly in aqueous contexts (29, 30). F^- is the smallest of the halides, with a radius approximately half an angstrom smaller than that of Cl^- (31). As such, F^- also has a higher charge density than Cl^- and is, therefore, an especially strong hydrogen bond acceptor. This is reflected in the high energetic cost to dehydrate fluoride, 111 kcal/mol, approximately 30 kcal/mol more costly than dehydration of Cl^- (32). Because the F^- ions are dehydrated for transport, this energetic barrier must be surmounted. Theoretical treatments of halides show that inner-sphere fluoride-water interactions are dominated by classical hydrogen bonds (33, 34), which are more tightly structured and closely held (35). In contrast, larger halides, including Cl^- , are more polarizable (36). Their coordination sphere is more flexible, and both hydrogen bond- and dipole-dominated configurations occur (34). F^- prefers approximately one to two fewer ligands than Cl^- (35, 37–39), and small-molecule hosts designed for fluoride recognition commonly use between four and six hydrogen bond donors (38). Another unique aspect of fluoride is that it is a stronger base than the other halides and pseudohalides (and its conjugate acid, HF, is a weaker acid). Whereas anions such as Cl^- and NO_3^- are exclusively ionized in aqueous media, the relatively high pK_a of HF means that this species may have relevance in biological systems, as it does in host-guest chemistry (11, 38). HF formation is particularly significant in low-dielectric environments such as the protein interior, where a F^- might share a proton with pK_a -matched side chains like aspartate or glutamate.

Thus, fluoride recognition by proteins is challenging due to the similar size of prominent biological competitors and the especially high free energy of dehydration. But there are also a number of physicochemical properties that membrane transport proteins could exploit to differentiate F^- from Cl^- , including the preference of fluoride for fewer ligands and a tighter coordination shell, its greater strength as a hydrogen bond acceptor, and its unique ability to share protons with pK_a -matched protonatable side chains.

CLC^F F⁻/H⁺ ANTIPTORTERS

When the fluoride riboswitches and associated genes were discovered, the CLC family of anion transport proteins was already well known to biology. The CLC family comprises both anion

Pseudohalide: a polyatomic anion that resembles the halides (fluoride, chloride, bromide, and iodide) in charge and chemical properties; examples include nitrate, thiocyanate, cyanate, and azide

channels and proton-coupled transporters and is broadly distributed among nearly all organisms and cell types. CLCs play diverse physiological roles ranging from extreme acid resistance in bacteria, acidification of intracellular vesicles in eukaryotes, maintenance of the resting membrane potential of skeletal muscle and of solute concentration in the kidney in animals, and generation of the voltage that electric rays use to electrocute their prey (40, 41). Although Cl^- is the namesake of the family and in most cases the physiological ion, the canonical CLC proteins are not very selective among anions and also permeate other halides and pseudohalides like iodide, bromide, and nitrate (42). A number of Cl^- -transporting CLCs have been structurally characterized, providing a deep mechanistic basis for understanding the fluoride riboswitch-associated CLCs (43–47).

The riboswitch-associated CLC proteins cluster together in a single bacterial clade of the CLC phylogeny (26). Not all proteins in this clade are associated with a riboswitch, but representatives with and without riboswitches share basic transport properties; the proteins in this clade were thus renamed CLC^{F} s (1). When heterologously expressed, CLC^{F} representatives from both gram-negative and gram-positive bacteria protect *E. coli* against fluoride toxicity (1). Genes encoding proteins in the CLC^{F} clade are overexpressed in fluoride-resistant *Streptococcus mutans* (48) and upregulated in *Enterococcus faecalis* in response to fluoride stress (49), and deletion of the CLC^{F} genes severely impairs growth of the oral bacteria *S. mutans* and *Streptococcus anginosus* in fluoride-containing media (50). In addition, a number of homologs have been purified and characterized using in vitro transport and electrophysiological assays. The transporters harness the transmembrane proton gradient to export one F^- in exchange for one H^+ , and the unitary transport rates of different characterized homologs range from ~ 400 to 1,000 ions/s (1, 51). Sequence alignments show that proteins in the CLC^{F} clade lack many of the essential chloride-coordinating residues that are well conserved in other chloride-transporting family members (1). In accord with this observation, the CLC^{F} s exhibit high selectivity for F^- relative to Cl^- , such that Cl^- permeation is not observed unless a high membrane potential is applied (1, 26, 51). Such selectivity is unique among CLCs but makes good physiological sense: Fluoride export is the only context described as yet in which a CLC must discriminate against monovalent anions that are more prevalent than the substrate in the biological milieu.

CLC^F Structure and Fluoride Coordination

Like other CLC proteins, CLC^{F} s assemble as homodimers (52, 53). Each monomer contains the necessary machinery for ion permeation and proton coupling, and if mutations are introduced that force the protein into a monomeric state, the lone subunits are capable of functioning independently (52). X-ray crystal structures of a CLC^{F} homolog from *Enterococcus casseliflavus* (53) show that each monomer possesses 14 transmembrane α -helices comprising two structurally homologous seven-helix domains that are related to one another by internal inverted symmetry (**Figure 3a,b**). In accordance with their role in anion transport, the α -helices are tilted with respect to the membrane, defining electropositive internal and external aqueous vestibules that are 6–8 Å deep (**Figure 3c**). Breaks in these helices position the positive helix dipoles of the N-terminal ends of the helices near the central dehydrated anion-binding region of the protein and also provide backbone amides to coordinate the transient anions (**Figure 3d**).

The crystal structures exhibit electron densities in two positions along the ion permeation pathway, termed the central (F_{cen}) and external (F_{ext}) anion-binding sites (53) (**Figure 3d**). Although fluoride is isoelectronic with water and thus indistinguishable by X-ray diffraction, these densities were assigned as F^- ions by analogy to the well-characterized permeation pathway of other CLC proteins. The first of the fluoride-binding sites, F_{cen} , sits at the apex of the cytoplasmic vestibule, where it is exposed to water and coordinated by protein side chains in a manner reminiscent of

Helix dipole: the sum of amino acid dipoles renders the α -helix positive at the amino end and negative at the carboxyl end

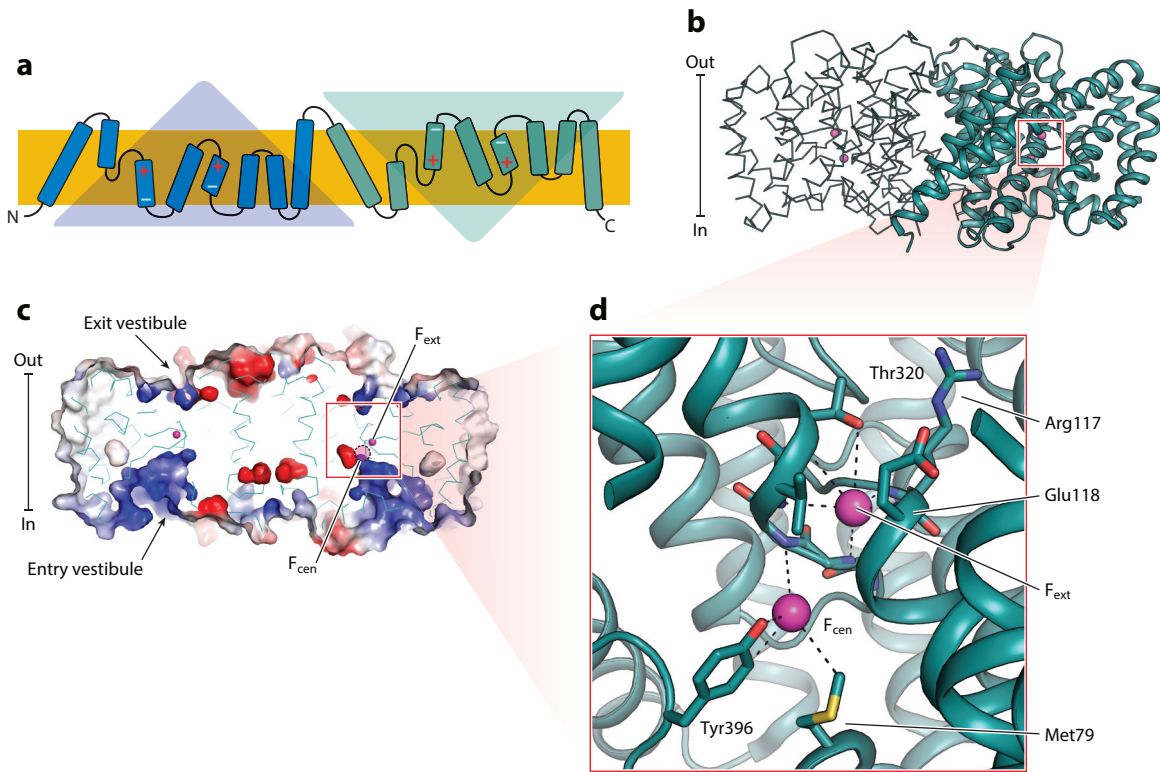


Figure 3

CLC^F architecture and F⁻ binding. (a) Transmembrane topology of a single subunit of the CLC^F dimer. The two domains of the inverted repeat are colored blue and teal. (b) Three-dimensional structure of the CLC^F dimer from *Enterococcus casseliflavus* (PDB ID 6D0J) with bound F⁻ ions and approximate membrane boundaries shown. (c) Side view of a CLC^F dimer sliced along a plane perpendicular to the membrane at the protein center, with the electrostatic surface shown. Blue regions are electropositive, and red regions are electronegative. F⁻ ions at the F_{ext} position are shown as pink spheres. F⁻ ions at the F_{cen} position are not visible in this slice; their approximate location at the top of the intracellular vestibule is indicated by the dashed circle. (d) Detailed view of fluoride binding at F_{cen} and F_{ext}. Amino acids within hydrogen-bond distance are shown as sticks, with potential hydrogen bonds shown as dashed lines. Abbreviations: F_{cen}, central anion-binding site; F_{ext}, external anion-binding site; PDB ID, Protein Data Bank identifier.

other CLCs. In an interaction that has precedent in the Cl⁻ transporters (43), a side chain hydroxyl from Y396 coordinates the fluoride. A methionine, M79, also contributes to F⁻ coordination via the terminal methyl group of the side chain, which is polarized and rendered weakly electropositive by the adjacent electron-withdrawing sulfur. Mutagenesis experiments showed that this methionine contributes to F⁻/Cl⁻ selectivity in the CLC^F proteins, and conversion to the straightforwardly polar asparagine reduces selectivity in a close homolog of the *E. casseliflavus* protein (51). The methionine is a somewhat surprising participant in fluoride coordination, since, in general, hard bases (like F⁻) prefer coordination by hard acids, like conventional hydrogen bond donors asparagine or serine (54). However, as described in the section titled Fluc F⁻ Channels, F⁻ coordination by polarizable amino acids, and methionine in particular, is reprised in the Fluc fluoride channels.

The second fluoride-binding site observed in the crystal structure, F_{ext}, is entirely dehydrated. This ion is coordinated by the side chain of T320 along with backbone amides from consecutive

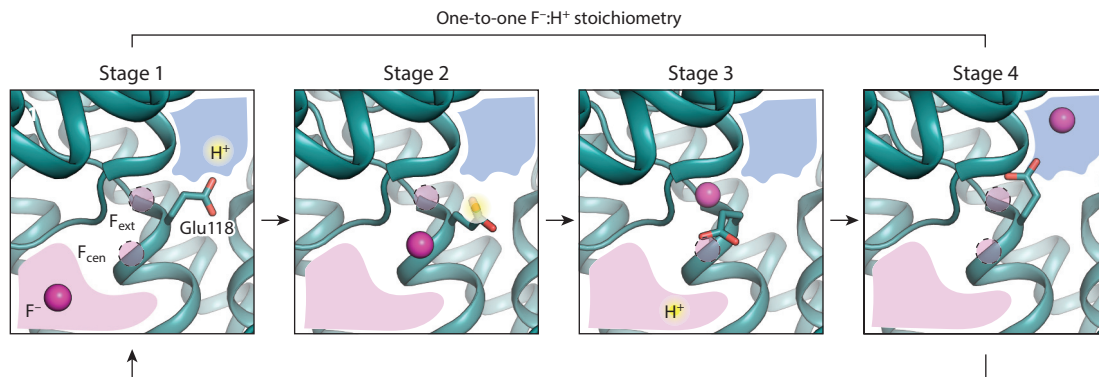


Figure 4

Proposed CLC^F transport mechanism. The extracellular solution is shown in blue and the intracellular solution in pink. The gating glutamate, E118, is shown in stick representation, and a yellow halo indicates protonation. In Stage 1, E118 is in the up position, where it can be protonated. In Stage 2, the now-neutral protonated E118 follows a hydrophobic pathway to the intracellular vestibule, bypassing the electropositive F^- binding sites. In Stage 3, E118 releases its proton to the intracellular vestibule. In the final stage (Stage 4), the deprotonated E118 transits along the F^- permeation route back to the extracellular vestibule, pushing a single F^- ion ahead of itself. F^- ions are shown as pink spheres, and unoccupied fluoride binding sites are indicated with pink dashed circles. Abbreviations: F_{cen} , central anion-binding site; F_{ext} , external anion-binding site.

residues, G116–G119, contributed by a helical break. In the structure of wild type CLC^F , F^- ions occupy both the F_{cen} and the dehydrated F_{ext} sites.

CLC^F Fluoride Transport Mechanism and Selectivity

In addition to the fluoride-coordinating residues, a final critical component of the transport machinery is the proton carrier E118, which faces the external solution in the structure of the wild type *E. casseliflavus* CLC^F . All members of the CLC family possess this so-called gating glutamate. In the CLC channels, the equivalent glutamate gates the conduction pathway depending on its protonation state (55), and in the CLC transporters, the glutamate participates in transport of the permeant H^+ (56–58). The gating glutamate is likewise a key mechanistic player in the transport cycle of CLC^F .

The CLC^F transport cycle proposed by Last, Miller, and colleagues (53) is based on competition between F^- and the negatively charged carboxylate of E118 for the binding sites F_{cen} and F_{ext} (Figure 4). In stage 1 of the transport cycle, the side chain of the gating glutamate E118 is in the up position, where it can obtain a proton from the extracellular milieu. Upon protonation, the now-neutral glutamate is proposed to swing down, following a hydrophobic pathway and bypassing the electropositive F^- binding sites (stage 2) so that it extends downward to access the intracellular vestibule, where it can release the bound proton to the cytoplasm (stage 3). Such a conformationally swapped state, with E118 exposed to the internal solution, was captured in the crystal structure of a mutant transporter, V319G (53).

In the final phase of the transport cycle, having deposited its proton on the intracellular side, the now-negatively charged E118 outcompetes F^- for the F_{cen} site, chasing the bound F^- along the permeation pathway toward the extracellular solution. Deprotonated E118 is proposed to follow the $F_{cen} \rightarrow F_{ext} \rightarrow$ external vestibule anion permeation route (stage 4), pushing a single F^- ahead of it, such that E118 transits back to the up position in the extracellular vestibule. Thus, the excursions of this single side chain carry a H^+ to the intracellular side, then electrostatically push a

F⁻ to the extracellular side, providing a structural explanation for the one-to-one F⁻/H⁺ exchange stoichiometry. In accord with the proposal that electrostatic repulsion by the E118 carboxylate hastens F⁻ along the permeation pathway, F⁻ transport is abolished in neutral mutants E118Q and E118A because the F⁻ binding affinity is over an order of magnitude higher in these mutants compared with wild type (51, 53). In the absence of F⁻, these mutants support Cl⁻ efflux, albeit uncoupled to H⁺ exchange (53).

Compared with other CLC transporters, the aqueous vestibules of CLC^F are deeper and the anhydrous zone crossed by the permeant ions is shorter. This may be an adaptation to prevent unproductive interactions between the gating glutamate and the permeant F⁻, which are close in pK_a and could conceivably capture a H⁺ between them, especially when traversing a long, low-dielectric span. As a mechanistic counterpoint to the CLC^Fs, a bacterial Cl⁻/H⁺ CLC antiporter is potently inhibited when the protonated gating glutamate hydrogen bonds with a F⁻ in the anion binding site, locking down the glutamate and interrupting the transport cycle (59, 60). Thus, although the CLC^F proteins share many mechanistic features with the large CLC family of Cl⁻ transporters, both the anion binding sites and the interactions between the fluoride and the gating glutamate have been optimized for F⁻ transduction.

FLUC F⁻ CHANNELS

The second family of membrane proteins associated with the fluoride riboswitches is entirely dedicated to fluoride transport, and its members are unlike any previously characterized protein. Genes encoding these proteins, originally called *crcB*, are found not only in bacteria but also in archaea, unicellular eukaryotes, fungi, plants, and filter-feeding ocean animals like sponges and sea anemones. Electrophysiological characterization showed that the proteins encoded by the *crcB* genes are electrodiffusive F⁻ channels (2, 3, 61–64), and they were renamed Fluc in bacteria and FEX in eukaryotes. Although it seems puzzling that a thermodynamically passive channel mechanism could protect organisms against external F⁻, two factors favor fluoride export in the physiological context. First, the weak acid accumulation effect can lead to cytoplasmic fluoride levels that exceed external F⁻, and a fluoride-selective efflux pathway simply undermines this process. Second, a metabolizing cell maintains a negative-inside membrane potential, so the electrical potential favors anion expulsion (15).

In harmony with an electrodiffusive mechanism, single Fluc channels can be monitored in planar lipid bilayer electrophysiological recordings, where the observed fluoride conductances correspond to a throughput of ~10⁵–10⁶ ions/s (2, 62). Unlike many gated channels, which open only in response to specific stimuli, the Fluc channels are constitutively open. However, the rapid fluoride conduction and lack of regulation pose a biophysical challenge: F⁻/Cl⁻ selectivity of 100-fold, or even 1,000-fold, would still permit an intolerable Cl⁻ leak. Accordingly, the Flucs are perhaps the most selective ion channels known; not even low levels of Cl⁻ transport are observed, placing the F⁻/Cl⁻ selectivity at a minimum of 10,000-fold (2).

The protective role of the fluoride channels has been demonstrated in a broad array of organisms. Knockouts of genomic Fluc/FEX proteins greatly increase the fluoride sensitivity of bacteria including *E. coli* (15, 26), *Bacillus subtilis* (26, 65), and the oral bacterium *Streptococcus sanguinis* (50); fungi including *Saccharomyces cerevisiae* (3, 27), *Candida albicans* (27), *Neurospora crassa* (27), and *Aspergillus fumigatus* (66); and the plant *Arabidopsis thaliana* (67). Heterologously expressed protein from an animal, the sea sponge *Amphimedon queenslandica* (68), complements strains of *S. cerevisiae* in which endogenous FEX channels have been knocked out. Since fluoride accumulation in tea leaves is a source of chronic endemic fluoride toxicity in many parts of the world (69), the

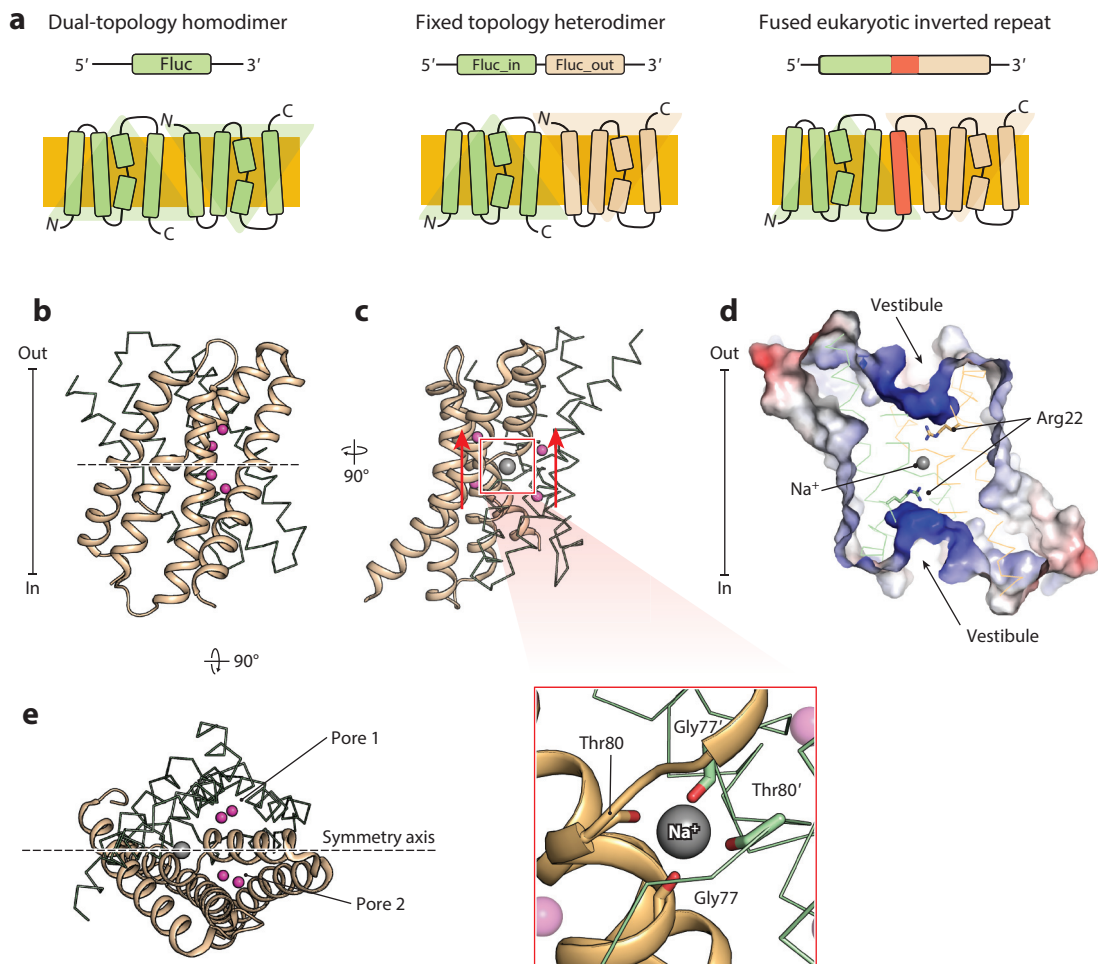


Figure 5

Fluoride channel (Fluc) architecture. (a) Fluoride channel topologies, including dual topology homodimers, antiparallel heterodimers, and inverted repeat monomers. The genetic architecture is shown at the top, and the resultant membrane topology is shown at the bottom. (b) Structure of Fluc-Bpe (PDB ID 5NKQ). One monomer is rendered in stick format and the other monomer in ribbon format. F⁻ ions are shown as pink spheres. The twofold symmetry axis is shown as a dashed line. (c, top) View of the Fluc dimer from panel b rotated 90° with the central Na⁺ shown as a gray sphere. Arrows adjacent to the F⁻ ions denote the direction of fluoride movement along the two pores. (c, bottom) Zoomed-in view of the central Na⁺ binding site with the backbone atoms of coordinating residues shown as sticks. (d) Fluc channel sliced at the midpoint along a plane perpendicular to the membrane with surface electrostatics shown. Electropositive surfaces are depicted in blue. (e) Top-down view of a Fluc homodimer with the twofold symmetry axis shown as a dashed line. Abbreviation: PDB ID, Protein Data Bank identifier.

expression and activity patterns of fluoride channels in various cultivars of the tea plant *Camellia sinensis* are also under scrutiny for their role in mitigating intracellular fluoride accumulation (67, 70).

Architecture of Fluoride Channels

The fluoride channel family encompasses a topologically diverse set of proteins that provide an unusual glimpse into evolutionary processes in membrane transport proteins (71) (**Figure 5a**).

Inverted repeat:

two structurally homologous domains in a single polypeptide arranged with antiparallel topology

Dual topology:

a membrane protein that is inserted into the membrane in both inward- and outward-facing orientations

The eukaryotic FEX proteins, like the CLC^F proteins, have an inverted repeat architecture, in which two structurally homologous domains in a single polypeptide are arranged in opposite orientations (3, 27). Many other diverse membrane protein folds share this construction, which presumably arose from the duplication and fusion of a primal homodimer (72, 73).

Remarkably, the bacterial Flucs embody this evolutionary antecedent, assembling as dual topology dimers with one subunit inserted into the membrane with the termini facing out and the other inserted into the membrane with the termini facing in (2, 61). Dual topology architecture was first predicted for the homodimeric Flucs by Rapp, von Heijne, and colleagues (74) years before their function was known, based on protein sequences alone. Such architecture is quite unusual, and although it has been proposed for several other membrane protein families (74), it has been structurally confirmed for only two other transporter classes (75, 76). For the Flucs, this rare architecture was experimentally confirmed via diverse approaches including crosslinking analysis, genetic fusion of the domains, a single-channel inhibitor binding assay, and solution of the three-dimensional structure (2, 61, 77). In addition to the dual topology homodimers, gene duplications have occurred among bacterial Flucs on at least five occasions (71); the resultant protomers assemble as obligate antiparallel heterodimers in which both subunits are required for channel assembly and function (2). The Flucs are the only functionally characterized family with modern-day representatives of all topological states along this evolutionary trajectory.

Of these various topologies, the dual topology homodimers from *Bordetella pertussis* (Fluc-Bpe) and an *E. coli* virulence plasmid (Fluc-Ec2) are the only ones that have been structurally characterized (64, 77, 78). The Fluc fold is unique among known membrane proteins. The two 15-kDa subunits in the dimer, each composed of four transmembrane helices known as TM1–4, adopt identical structures such that the channels possess twofold symmetry about an axis parallel to the plane of the membrane (**Figure 5b**). TM3 has a five-residue helical break that corresponds to one of the most highly conserved sequences in the protein. When the dimer is assembled, the TM3 breaks cross over each other at the heart of the protein, where free backbone carbonyl oxygens coordinate a central Na⁺ at the dimer interface (**Figure 5c**). This structural Na⁺ is deeply buried, stably bound, and likely inserted upon dimer assembly (79). Although there is no known precedent among membrane proteins for such a nontransported structural Na⁺, the binding site on the symmetry axis, coordinated by backbone carbonyl oxygens, resembles some Na⁺ binding sites in Na⁺-coupled transporters (79).

The channel adopts a symmetrical hourglass shape with wide aqueous vestibules on both sides of the membrane (**Figure 5d**). These vestibules are separated by a 10-Å-thick protein plug that houses the structural Na⁺. This Na⁺ and a universally conserved arginine residue, R22, render the vestibules electropositive, and both R22 and the Na⁺ are essential for fluoride permeation (79). As a consequence of the dual topology architecture and twofold symmetry, structural features that lie off the symmetry axis are found in duplicate. For example, the cytoplasmic and periplasmic faces of the channel are structurally identical. Functional experiments support this observation: An inhibitor applied in sequence to the *cis* and *trans* sides of a single Fluc channel in a planar lipid bilayer blocks both sides of the channel with identical kinetics (61–63). More strikingly, the channel also possesses a duplicate set of pores, each demarcated by a pair of F⁻ ions arranged vertically, slightly off normal to the membrane plane (**Figure 5c,e**). Although the twofold symmetry of the channels dictates that the two pores are antiparallel with respect to each other, electrophysiological experiments showed that fluoride uses both conduits to flow down its electrochemical gradient (80). However, inspection of the sequences of the heterodimeric and inverted-repeat fluoride channels suggests that the presence of both pores is not necessary. In the heterodimeric Fluc and FEX proteins, essential pore-lining residues are conserved in only one of the two domains

(3, 68, 77), providing a case study in how redundant features degrade upon gene duplication, fusion, and genetic drift.

Fluc Fluoride Coordination and Proposed Permeation Pathway

Using a combination of crystallographic and functional data from Fluc-Bpe and Fluc-Ec2, three different F⁻ binding sites have been proposed along the permeation pathway. **Figure 6a** and **6b** illustrate the proposed pore and are built from several different structures of the two homologs. **Figure 6b** posits a mechanism of alternating fluoride site occupancy, akin to that described for other multi-ion channels (81–85), where electrostatic repulsion between ions in adjacent sites contributes to rapid ion throughput. For simplicity, the panels in **Figure 6** show Fluc-Bpe unless otherwise indicated, residue numbering corresponds to Fluc-Bpe, and only one of the two structurally identical pores is described.

F⁻ ions are proposed to accumulate in the electropositive vestibule, and in agreement with this, F⁻ currents are inhibited if the vestibule is occluded by the bulky, negatively charged thiol-reactive reagent 2-[(methylsulfonyl)thio]-ethanesulfonic acid (MTSES) (85a). The first binding site along the permeation pathway, denoted F₀, is located at the bottom of the vestibule. This site is nonspecific among anions and was first identified by cocrystallization of Fluc-Ec2 with bromide (Br⁻), a halide that anomalously scatters X-ray beams (85a). An anion in the F₀ site is coordinated by the side chain hydroxyl groups of two highly conserved residues from the TM3 break, S83 and T84, along with bulk vestibule solvent. These positions are sensitive to mutagenesis: S83C and S83T are incompetent for F⁻ transport, and the double S83A/T84A mutant exhibits currents just 1% of wild type (85a). Such aqueous entryways are familiar features of ion channels more generally and function to increase the rate of ion entry into the channel before the ions proceed to the constricted selectivity filter (86–88).

From F₀, the F⁻ ion is proposed to move laterally to access the fluoride-selective binding site F₁, which is located in an anhydrous crevice between TM2, TM3a, and TM4. F₁ and the next binding site in the series, F₂, delineate a pathway that runs perpendicular to the membrane along one face of TM4. Termed the polar track, this stretch of sequence is defined by a hydrogen bond donor at every fourth position, or one per helical turn (indicated with asterisks in **Figure 6a**). Sequence alignments show that although the identity of the polar-track residues is not conserved among Fluc proteins, the polar, hydrogen bond-donating nature is (**Figure 6c**). In addition, TM2 contributes a completely conserved hydrogen bond donor, N43, to this polar, dehydrated stretch. N43 is situated between F₁ and F₂ with the side chain amide coordinating F₂. A rotameric switch would bring this side chain within coordination distance of F₁, and such an event was conjectured to be part of the transport mechanism (77). Alteration of N43 typically eliminates fluoride transport entirely (77, 89); the polar-track residues, like the side chains that coordinate F₀, are somewhat more tolerant of alanine substitution (89).

Along with this enrichment of hydrogen bond donors, the transient F⁻ ions in the F₁ and F₂ positions are also coordinated by the electropositive edges of a pair of phenylalanines, F82 and F85 (**Figure 6d**). These highly conserved side chains are arranged adjacent to the polar track in a symmetrical box configuration, with the electropositive edge of each phenylalanine adjacent to the electronegative face of the next phenylalanine. The polarizable aromatic rings are positioned to interact with the fluoride densities via side-on coordination by the electropositive quadrupoles of the ring edges. Such interactions, termed anion-quadrupole interactions, have been observed in a variety of macromolecular contexts and also occur between F⁻ and aromatic rings in small molecules (90–92). Mutation of either F82 or F85 to a nonpolarizable hydrophobic residue like isoleucine greatly reduces or abolishes F⁻ transport, depending on the homolog (77, 80). Mutation

Selectivity filter: the narrowest portion of an ion channel's conduction pathway that discriminates between ions

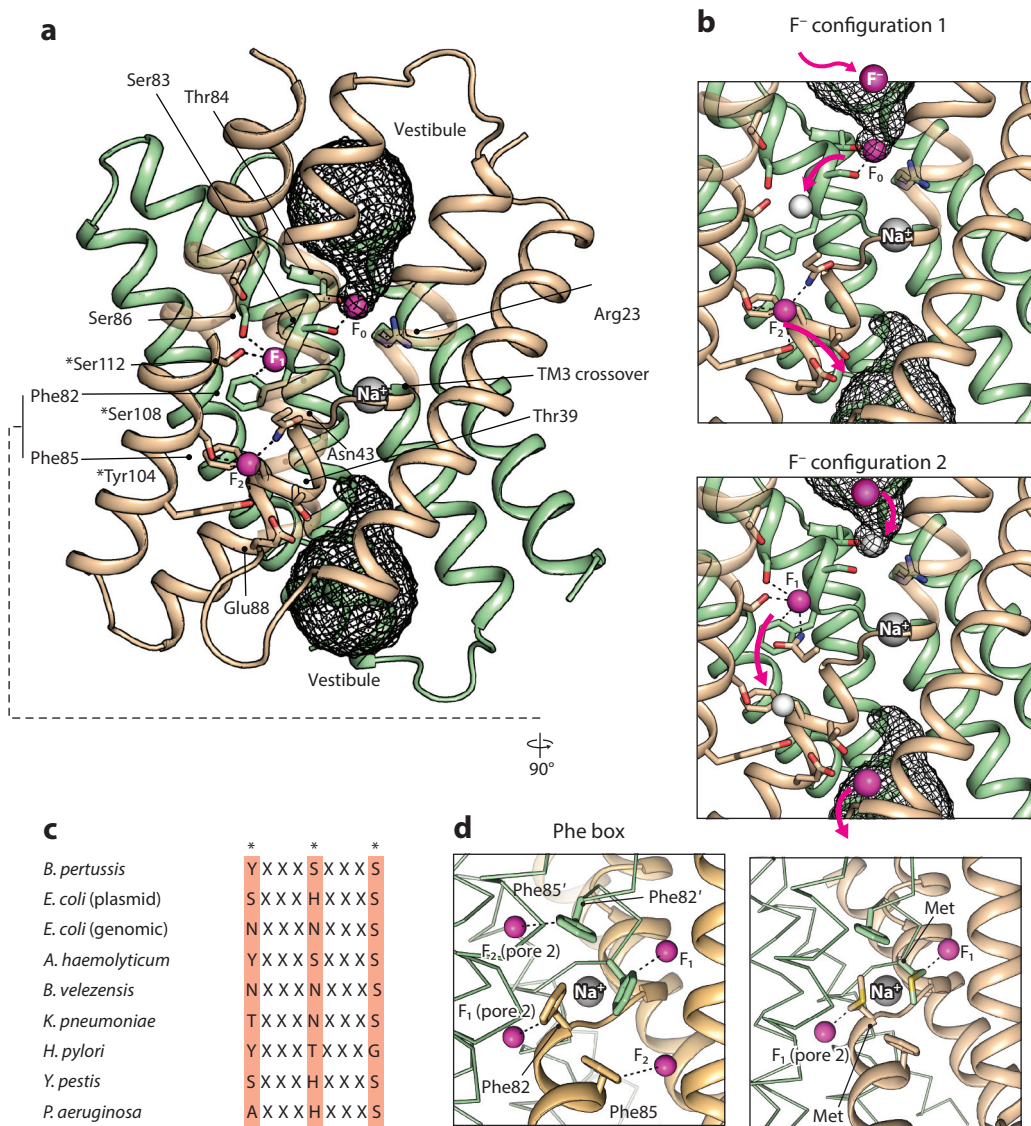


Figure 6

Proposed fluoride channel pore. (a) Compilation of structural data from Fluc-Bpe and Fluc-Ec2 showing fluoride binding sites F_0 , F_1 , and F_2 along the proposed fluoride permeation pathway. Numbering corresponds to Fluc-Bpe, with mechanistically important side chains shown as sticks and polar track residues indicated by asterisks. Subunits are colored tan and green with aqueous vestibules [determined by CAVER (102)] shown as dark mesh. (b) Proposed alternate occupancy of F^- ions. The electrostatic repulsion that occurs between F^- ions in adjacent sites contributes to rapid conduction. Zoomed-in views of fluoride binding configurations with occupied sites are indicated in pink and unoccupied sites in white. F^- movement is indicated with pink arrows. (c) Sequence alignment of the transmembrane helix TM4 polar track of microbial Fluc channels from *Bordetella pertussis*, *Escherichia coli*, *Arcanobacterium haemolyticum*, *Bacillus velezensis*, *Klebsiella pneumoniae*, *Helicobacter pylori*, *Yersinia pestis*, and *Pseudomonas aeruginosa*. (d, left) View of the phenylalanine box with edge-on coordination of F^- ions indicated with dashed lines. This view emphasizes the two-pore construction of the channel. Note that in panels a and d, the ions in the F_1 -pore 2 and F_2 -pore 2 sites are omitted for clarity. (d, right) Structure of Fluc-Ec2 mutant F82M (PDB ID 6B2B), a fluoride-conducting phenylalanine-box mutant. Abbreviation: PDB ID, Protein Data Bank identifier.

to polar aromatic side chains like tyrosine and tryptophan does not support transport either (89). However, mutation to methionine, which, like phenylalanine, is both hydrophobic and polarizable, supports fluoride conductance at wild type levels (89). The structure of this mutant shows that the substituted methionine adopts a twisted conformation, filling approximately the same space as the phenylalanine ring in the wild type protein, with the electropositive γ -methylene sitting in the same position as the phenylalanine edge (**Figure 6d**). This interaction calls to mind the CLC^{F} 's coordination of F_{cen} by a methionine, and in a handful of bacterial Fluc homologs, the phenylalanine-box sequence motif includes a methionine instead (89).

After visiting sites F_0 , F_1 , and F_2 , the permeant F^- is presumed to exit the pore on the other side of the membrane, near the mouth of the opposite vestibule. At this position resides a glutamate, E88. This glutamate is extremely well conserved among fluoride channels and follows the same pattern of conservation and degradation in the different domains of the eukaryotic channels as other pore-lining residues (77). In *S. cerevisiae* FEX channels, mutation of the corresponding glutamate renders the protein unprotective against F^- (68). Some evidence suggests that E88 contributes to anion selectivity, although its exact role is unclear. Analogy to the CLC^{F} proteins suggests the interesting hypothesis that E88 hastens F^- dissociation with an electrostatic push.

Anion-quadrupole interaction:
noncovalent interaction between an anion and the electron-deficient edge of an aromatic ring

The Unresolved Question of Fluoride Selectivity by the Flucs

Although the permeation pathway has been determined, the features responsible for the striking 10,000-fold F^-/Cl^- selectivity have not yet been identified. Of dozens of mutations, none have allowed substantial throughput of any other anion, and increasing the bore of the channel by paring back side chains has not yet been shown to decrease selectivity (77, 79, 80, 89). Because F^- requires the smallest number of coordinating ligands of any anion, it is plausible that only by adding ligands to the fluoride-binding sites could the channel be engineered to bind other anions. Such a maneuver would be difficult or impossible by site-directed mutagenesis alone. This type of selectivity mechanism, based on optimizing the number of protein ligands to coordinate the physiological ion and exclude competing ions, has been proposed for K^+ channels (93, 94) and as a general ion selectivity principle (35). The proposed fluoride-binding sites in Fluc may be undercoordinated, with few protein ligands (three or four are observed in the structures, assuming limited side chain rearrangement), in order to exclude Cl^- . This sparsity of ligands in Fluc draws a contrast with the five to six ligands provided to each anion-binding site by the less-selective CLC^{F} s. It is also possible that rather than one selectivity filter, the Fluc channels have evolved multiple selectivity checkpoints, such that mutation to multiple regions of the protein would be required to permit chloride conduction. Or it could be that some molecular feature—perhaps the hydrophobic polarizable side chains—presents an insurmountable kinetic barrier to permeation by softer anions. Whatever the biophysical basis, the Flucs are impeccably optimized for fluoride selectivity and rapid conduction, all accomplished without any depletion of the microbe's energy stores. It seems significant that the Fluc family has not evolved into a diversity of physiological roles like the CLCs: The Flucs are very specialized in what they do.

CONCLUSIONS

Nature has independently evolved two strikingly different fluoride export proteins to solve the problem of cytoplasmic fluoride accumulation. Not only do the proteins possess unrelated folds, but also, it is highly unusual for the same biological problem to be solved by both passive and active transport mechanisms. Despite their very obvious differences in form and function, the CLC^{F} and Fluc proteins also share some common features. Some of these are expected, like the

prevalence of hydroxyl side chains as hydrogen bond donors for fluoride. Other common features are more surprising, like the involvement of hydrophobic, polarizable side chains of methionine and phenylalanine in F^- coordination and the presence of mechanistically important glutamate side chains along the fluoride transport pathway. It remains to be determined whether the convergence of these features in the CLC^F s and fluoride channels is evolutionary happenstance or whether it reflects the unique suitability of these residues for fluoride conduction.

SUMMARY POINTS

1. F^- is ubiquitous in terrestrial and aquatic environments and poses a threat to microbes because it can accumulate in the cytoplasm via a weak acid ion-trapping mechanism, where it inhibits diverse metalloenzymes.
2. Two strikingly different families of membrane proteins export cytoplasmic fluoride: the $CLC^F F^-/H^+$ antiporters and the Fluc fluoride channels.
3. CLC^F transporters are a fluoride-specialized variant of the ubiquitous CLC family of anion channels and transporters.
4. The Fluc family is dedicated to F^- export and has a unique structure among membrane proteins. However, fundamental aspects of its construction call to mind features of long-studied ion channels, including the wide aqueous entryway (86–88) and multi-ion conduction (81–85).
5. Although they are structurally unrelated, the CLC^F s and Flucs share common features in their F^- permeation pathways, including coordination by hydrophobic, polarizable amino acids such as methionine and phenylalanine; hydrogen bond donation by hydroxyl side chains; and participation of conserved glutamate residues.

FUTURE ISSUES

1. Additional mechanistic work, including both experimental and computational investigations, is important to understand the contributions of polarizable amino acids to F^- binding and the physicochemical basis of F^- selectivity, especially in the Flucs, for which no modification has yet been discovered that permits the permeation of any other anion.
2. Eukaryotic FEX proteins have a fundamental architectural difference from the homodimeric Flucs. Structural characterization of eukaryotic FEX proteins is important both to understand how eukaryotic pathogens resist environmental fluoride and to answer more basic questions about how membrane proteins evolve in complexity upon duplication and fusion of the individual subunits.
3. Identification of the microbial molecular response to fluoride has launched a new era in applied fluoride physiology, including the use of fluoride channels as selectable markers in transgenic yeast (95), the design of fluoride-centric antimicrobial approaches (96), and the engineering of tea cultivars to decrease fluoride accumulation (67). Research is ongoing in a variety of organisms relevant to human disease to understand whether fluoride-sensing and fluoride export systems are suitable drug targets, particularly in dental applications (66, 97, 98).

4. It remains unknown whether higher animals, including mammals, possess fluoride export proteins. Although fluoride is not transported to the bloodstream by the excretory epithelia, epithelial cells in the gut are exposed to this halide, and the molecular physiology of these encounters, including any possible export system, is still unknown.

DISCLOSURE STATEMENT

The authors are not aware of any affiliations, memberships, funding, or financial holdings that might be perceived as affecting the objectivity of this review.

ACKNOWLEDGMENTS

We thank members of the Stockbridge lab, especially Jason Devlin and Rachael Lucero, for comments on the manuscript. This work was supported by National Institutes of Health grant R35 GM128768 to R.B.S.

LITERATURE CITED

1. Stockbridge RB, Lim HH, Otten R, Williams C, Shane T, et al. 2012. Fluoride resistance and transport by riboswitch-controlled CLC antiporters. *PNAS* 109:15289–94
2. Stockbridge RB, Robertson JL, Kolmakova-Partensky L, Miller C. 2013. A family of fluoride-specific ion channels with dual-topology architecture. *eLife* 2:e01084
3. Smith KD, Gordon PB, Rivetta A, Allen KE, Berbasova T, et al. 2015. Yeast Fex1p is a constitutively expressed fluoride channel with functional asymmetry of its two homologous domains. *J. Biol. Chem.* 290:19874–87
4. Weinstein LH, Davison A. 2004. *Fluorides in the Environment: Effects on Plants and Animals*. Cambridge, MA: CABI Publ.
5. Jagtap S, Yenkie MK, Labhsetwar N, Rayalu S. 2012. Fluoride in drinking water and defluoridation of water. *Chem. Rev.* 112:2454–66
6. Windom HL. 1971. Fluoride concentration in coastal and estuarine waters of Georgia. *Limnol. Oceanogr.* 16:806–10
7. U.S. Dep. Health Hum. Serv. Fed. Panel Community Water Fluorid. 2015. U.S. Public Health Service recommendation for drinking water for the prevention of dental caries. *Public Health Rep.* 130:318–31
8. CDC (Cent. Dis. Control Prev.). My Water's Fluoride web application. *CDC Div. Oral Health*. https://nccd.cdc.gov/DOH_MWF/Default/Default.aspx
9. Johnston NR, Strobel SA. 2020. Principles of fluoride toxicity and the cellular response: a review. *Arch. Toxicol.* 94:1051–69
10. Barbier O, Arreola-Mendoza L, Del Razo LM. 2010. Molecular mechanisms of fluoride toxicity. *Chem. Biol. Interact.* 188:319–33
11. Orabi EA, Faraldo-Gomez JD. 2020. A new molecular-mechanics model for simulations of hydrogen fluoride in chemistry and biology. *J. Chem. Theory Comput.* 16:5105–26
12. Wilks JC, Slonczewski JL. 2007. pH of the cytoplasm and periplasm of *Escherichia coli*: rapid measurement by green fluorescent protein fluorimetry. *J. Bacteriol.* 189:5601–7
13. Krulwich TA, Sachs G, Padan E. 2011. Molecular aspects of bacterial pH sensing and homeostasis. *Nat. Rev. Microbiol.* 9:330–43
14. Marquis RE, Clock SA, Mota-Meira M. 2003. Fluoride and organic weak acids as modulators of microbial physiology. *FEMS Microbiol. Rev.* 26:493–510
15. Ji C, Stockbridge RB, Miller C. 2014. Bacterial fluoride resistance, Fluc channels, and the weak acid accumulation effect. *J. Gen. Physiol.* 144:257–61

16. Adamek E, Pawlowska-Goral K, Bober K. 2005. In vitro and in vivo effects of fluoride ions on enzyme activity. *Ann. Acad. Med. Stetin.* 51:69–85
17. Johnston NR, Strobel SA. 2019. Nitrate and phosphate transporters rescue fluoride toxicity in yeast. *Chem. Res. Toxicol.* 32:2305–19
18. Samygin VR, Moiseev VM, Rodina EV, Vorobyeva NN, Popov AN, et al. 2007. Reversible inhibition of *Escherichia coli* inorganic pyrophosphatase by fluoride: trapped catalytic intermediates in cryocrystallographic studies. *J. Mol. Biol.* 366:1305–17
19. Heikinheimo P, Tuominen V, Ahonen AK, Teplyakov A, Cooperman BS, et al. 2001. Toward a quantum-mechanical description of metal-assisted phosphoryl transfer in pyrophosphatase. *PNAS* 98:3121–26
20. Qin J, Chai G, Brewer JM, Lovelace LL, Lebioda L. 2006. Fluoride inhibition of enolase: crystal structure and thermodynamics. *Biochemistry* 45:793–800
21. Lebioda L, Zhang E, Lewinski K, Brewer JM. 1993. Fluoride inhibition of yeast enolase: crystal structure of the enolase-Mg²⁺-F⁻-P_i complex at 2.6 Å resolution. *Proteins* 16:219–25
22. Nowak T, Maurer PJ. 1981. Fluoride inhibition of yeast enolase. 2. Structural and kinetic properties of the ligand complexes determined by nuclear relaxation rate studies. *Biochemistry* 20:6901–11
23. Maurer PJ, Nowak T. 1981. Fluoride inhibition of yeast enolase. 1. Formation of the ligand complexes. *Biochemistry* 20:6894–900
24. Matte A, Tari LW, Delbaere LT. 1998. How do kinases transfer phosphoryl groups? *Structure* 6:413–19
25. Alani E, Lee JY, Schofield MJ, Kijas AW, Hsieh P, Yang W. 2003. Crystal structure and biochemical analysis of the MutS-ADP-beryllium fluoride complex suggests a conserved mechanism for ATP interactions in mismatch repair. *J. Biol. Chem.* 278:16088–94
26. Baker JL, Sudarsan N, Weinberg Z, Roth A, Stockbridge RB, Breaker RR. 2012. Widespread genetic switches and toxicity resistance proteins for fluoride. *Science* 335:233–35
27. Li S, Smith KD, Davis JH, Gordon PB, Breaker RR, Strobel SA. 2013. Eukaryotic resistance to fluoride toxicity mediated by a widespread family of fluoride export proteins. *PNAS* 110:19018–23
28. Schultz SG, Wilson NL, Epstein W. 1962. Cation transport in *Escherichia coli*. II. Intracellular chloride concentration. *J. Gen. Physiol.* 46:159–66
29. Cametti M, Rissanen K. 2009. Recognition and sensing of fluoride anion. *Chem. Commun.* 2009:2809–29
30. Clarke HJ, Howe EN, Wu X, Sommer F, Yano M, et al. 2016. Transmembrane fluoride transport: direct measurement and selectivity studies. *J. Am. Chem. Soc.* 138:16515–22
31. Shannon RD. 1976. Revised effective ionic radii and systematic studies of interatomic distances in halides and chalcogenides. *Acta Crystallogr. A* 32:751–67
32. Marcus Y. 1994. A simple empirical model describing the thermodynamics of hydration of ions of widely varying charges, sizes, and shapes. *Biophys. Chem.* 51:111–27
33. Muralidharan A, Pratt LR, Chaudhari MI, Rempe SB. 2018. Quasi-chemical theory with cluster sampling from ab initio molecular dynamics: fluoride (F⁻) anion hydration. *J. Phys. Chem. A* 122:9806–12
34. Muralidharan A, Pratt LR, Chaudhari MI, Rempe SB. 2019. Quasi-chemical theory for anion hydration and specific ion effects: Cl⁻ (aq) versus F⁻ (aq). *Chem. Phys. Lett. X* 4:100037
35. Bostick DL, Brooks CL. 2009. Statistical determinants of selective ionic complexation: ions in solvent, transport proteins, and other “hosts.” *Biophys. J.* 96:4470–92
36. Li M, Zhuang B, Lu Y, Wang ZG, An L. 2017. Accurate determination of ion polarizabilities in aqueous solutions. *J. Phys. Chem. B* 121:6416–24
37. Ohtaki H, Radnai T. 1993. Structure and dynamics of hydrated ions. *Chem. Rev.* 93:1157–204
38. Cametti M, Rissanen K. 2013. Highlights on contemporary recognition and sensing of fluoride anion in solution and in the solid state. *Chem. Soc. Rev.* 42:2016–38
39. Merchant S, Asthagiri D. 2009. Thermodynamically dominant hydration structures of aqueous ions. *J. Chem. Phys.* 130:195102
40. Jentsch TJ, Pusch M. 2018. CLC chloride channels and transporters: structure, function, physiology, and disease. *Physiol. Rev.* 98:1493–590
41. Miller C. 2015. In the beginning: a personal reminiscence on the origin and legacy of ClC-0, the ‘*Torpedo* Cl⁻ channel’. *J. Physiol.* 593:4085–90
42. Accardi A, Lobet S, Williams C, Miller C, Dutzler R. 2006. Synergism between halide binding and proton transport in a CLC-type exchanger. *J. Mol. Biol.* 362:691–99

43. Dutzler R, Campbell EB, Cadene M, Chait BT, MacKinnon R. 2002. X-ray structure of a ClC chloride channel at 3.0 Å reveals the molecular basis of anion selectivity. *Nature* 415:287–94
44. Jayaram H, Accardi A, Wu F, Williams C, Miller C. 2008. Ion permeation through a Cl⁻-selective channel designed from a ClC Cl⁻/H⁺ exchanger. *PNAS* 105:11194–99
45. Feng L, Campbell EB, Hsiung Y, MacKinnon R. 2010. Structure of a eukaryotic ClC transporter defines an intermediate state in the transport cycle. *Science* 330:635–41
46. Park E, Campbell EB, MacKinnon R. 2017. Structure of a ClC chloride ion channel by cryo-electron microscopy. *Nature* 541:500–5
47. Park E, MacKinnon R. 2018. Structure of the ClC-1 chloride channel from *Homo sapiens*. *eLife* 7:e36629
48. Liao Y, Chen J, Brandt BW, Zhu Y, Li J, et al. 2015. Identification and functional analysis of genome mutations in a fluoride-resistant *Streptococcus mutans* strain. *PLOS ONE* 10:e0122630
49. Li G, Shi M, Zhao S, Li D, Long Y, et al. 2020. RNA-Seq comparative analysis reveals the response of *Enterococcus faecalis* TV4 under fluoride exposure. *Gene* 726:144197
50. Men X, Shibata Y, Takeshita T, Yamashita Y. 2016. Identification of anion channels responsible for fluoride resistance in oral streptococci. *PLOS ONE* 11:e0165900
51. Brammer AE, Stockbridge RB, Miller C. 2014. F⁻/Cl⁻ selectivity in ClC^F-type F⁻/H⁺ antiporters. *J. Gen. Physiol.* 144:129–36
52. Last NB, Miller C. 2015. Functional monomerization of a ClC-type fluoride transporter. *J. Mol. Biol.* 427:3607–12
53. Last NB, Stockbridge RB, Wilson AE, Shane T, Kolmakova-Partensky L, et al. 2018. A ClC-type F⁻/H⁺ antiporter in ion-swapped conformations. *Nat. Struct. Mol. Biol.* 25:601–6
54. Pearson RG. 1966. Acids and bases. *Science* 151:172–77
55. Lisal J, Maduke M. 2008. The ClC-0 chloride channel is a ‘broken’ Cl⁻/H⁺ antiporter. *Nat. Struct. Mol. Biol.* 15:805–10
56. Feng L, Campbell EB, MacKinnon R. 2012. Molecular mechanism of proton transport in ClC Cl⁻/H⁺ exchange transporters. *PNAS* 109:11699–704
57. Dutzler R, Campbell EB, MacKinnon R. 2003. Gating the selectivity filter in ClC chloride channels. *Science* 300:108–12
58. Chavan TS, Cheng RC, Jiang T, Mathews II, Stein RA, et al. 2020. A ClC-ec1 mutant reveals global conformational change and suggests a unifying mechanism for the ClC Cl⁻/H⁺ transport cycle. *eLife* 9:e53479
59. Lim HH, Stockbridge RB, Miller C. 2013. Fluoride-dependent interruption of the transport cycle of a ClC Cl⁻/H⁺ antiporter. *Nat. Chem. Biol.* 9:721–25
60. Chiariello MG, Bolnykh V, Ippoliti E, Meloni S, Olsen JMH, et al. 2020. Molecular basis of ClC antiporter inhibition by fluoride. *J. Am. Chem. Soc.* 142:7254–58
61. Stockbridge RB, Koide A, Miller C, Koide S. 2014. Proof of dual-topology architecture of Fluc F⁻ channels with monobody blockers. *Nat. Commun.* 5:5120
62. Turman DL, Nathanson JT, Stockbridge RB, Street TO, Miller C. 2015. Two-sided block of a dual-topology F⁻ channel. *PNAS* 112:5697–701
63. Turman DL, Stockbridge RB. 2017. Mechanism of single- and double-sided inhibition of dual topology fluoride channels by synthetic monobodies. *J. Gen. Physiol.* 149:511–22
64. McIlwain BC, Newstead S, Stockbridge RB. 2018. Cork-in-bottle occlusion of fluoride ion channels by crystallization chaperones. *Structure* 26:635–39.e1
65. Dong W, Setlow P. 2019. Fluoride movement into and out of *Bacillus* spores and growing cells and effects of fluoride accumulation on spore properties. *J. Appl. Microbiol.* 126:503–15
66. Binder J, Held J, Krappmann S. 2019. Impairing fluoride export of *Aspergillus fumigatus* mitigates its voriconazole resistance. *Int. J. Antimicrob. Agents* 53:689–93
67. Song J, Hou C, Guo J, Niu Q, Wang X, et al. 2020. Two new members of CsFEXs couple proton gradients to export fluoride and participate in reducing the fluoride accumulation in low-fluoride tea cultivars. *J. Agric. Food Chem.* 68:8568–79
68. Berbasova T, Nallur S, Sells T, Smith KD, Gordon PB, et al. 2017. Fluoride export (FEX) proteins from fungi, plants and animals are ‘single barreled’ channels containing one functional and one vestigial ion pore. *PLOS ONE* 12:e0177096

69. Izuora K, Twombly JG, Whitford GM, Demertzis J, Pacifici R, Whyte MP. 2011. Skeletal fluorosis from brewed tea. *J. Clin. Endocrinol. Metab.* 96:2318–24
70. Zhu J, Xing A, Wu Z, Tao J, Ma Y, et al. 2019. CsFEX, a fluoride export protein gene from *Camellia sinensis*, alleviates fluoride toxicity in transgenic *Escherichia coli* and *Arabidopsis thaliana*. *J. Agric. Food Chem.* 67:5997–6006
71. Macdonald CB, Stockbridge RB. 2017. A topologically diverse family of fluoride channels. *Curr. Opin. Struct. Biol.* 45:142–49
72. Forrest LR. 2015. Structural symmetry in membrane proteins. *Annu. Rev. Biophys.* 44:311–37
73. Keller R, Ziegler C, Schneider D. 2014. When two turn into one: evolution of membrane transporters from half modules. *Biol. Chem.* 395:1379–88
74. Rapp M, Granseth E, Seppala S, von Heijne G. 2006. Identification and evolution of dual-topology membrane proteins. *Nat. Struct. Mol. Biol.* 13:112–16
75. Ubarretxena-Belandia I, Baldwin JM, Schuldiner S, Tate CG. 2003. Three-dimensional structure of the bacterial multidrug transporter EmrE shows it is an asymmetric homodimer. *EMBO J.* 22:6175–81
76. Assur Sanghai Z, Liu Q, Clarke OB, Belcher-Dufrisque M, Wiriyaermluk P, et al. 2018. Structure-based analysis of CysZ-mediated cellular uptake of sulfate. *eLife* 7:e27829
77. Stockbridge RB, Kolmakova-Partensky L, Shane T, Koide A, Koide S, et al. 2015. Crystal structures of a double-barrelled fluoride ion channel. *Nature* 525:548–51
78. Turman DL, Cheloff AZ, Corrado AD, Nathanson JT, Miller C. 2018. Molecular interactions between a fluoride ion channel and synthetic protein blockers. *Biochemistry* 57:1212–18
79. McIlwain BC, Martin K, Hayter EA, Stockbridge RB. 2020. An interfacial sodium ion is an essential structural feature of Fluc family fluoride channels. *J. Mol. Biol.* 432:1098–108
80. Last NB, Kolmakova-Partensky L, Shane T, Miller C. 2016. Mechanistic signs of double-barreled structure in a fluoride ion channel. *eLife* 5:e18767
81. Morais-Cabral JH, Zhou Y, MacKinnon R. 2001. Energetic optimization of ion conduction rate by the K⁺ selectivity filter. *Nature* 414:37–42
82. Hodgkin AL, Keynes RD. 1955. The potassium permeability of a giant nerve fibre. *J. Physiol.* 128:61–88
83. Eisenman W. 1962. A two-way affair. *Science* 136:182
84. Hille B, Schwarz W. 1978. Potassium channels as multi-ion single-file pores. *J. Gen. Physiol.* 72:409–42
85. Zhou YF, MacKinnon R. 2003. The occupancy of ions in the K⁺ selectivity filter: Charge balance and coupling of ion binding to a protein conformational change underlie high conduction rates. *J. Mol. Biol.* 333:965–75
- 85a. McIlwain BC, Gundepudi R, Koff BB, Stockbridge RB. The fluoride permeation pathway and anion recognition in Fluc family fluoride channels. bioRxiv 2021.04.03.438337. <https://doi.org/10.1101/2021.04.03.438337>
86. Doyle DA, Morais Cabral J, Pfuetzner RA, Kuo A, Gulbis JM, et al. 1998. The structure of the potassium channel: molecular basis of K⁺ conduction and selectivity. *Science* 280:69–77
87. Latorre R, Miller C. 1983. Conduction and selectivity in potassium channels. *J. Membr. Biol.* 71:11–30
88. Payandeh J, Scheuer T, Zheng N, Catterall WA. 2011. The crystal structure of a voltage-gated sodium channel. *Nature* 475:353–58
89. Last NB, Sun S, Pham MC, Miller C. 2017. Molecular determinants of permeation in a fluoride-specific ion channel. *eLife* 6:e31259
90. Philip V, Harris J, Adams R, Nguyen D, Spiers J, et al. 2011. A survey of aspartate-phenylalanine and glutamate-phenylalanine interactions in the Protein Data Bank: searching for anion- π pairs. *Biochemistry* 50:2939–50
91. Allen FH. 2002. The Cambridge Structural Database: a quarter of a million crystal structures and rising. *Acta Crystallogr. B* 58:380–88
92. Chakravarty S, Ung AR, Moore B, Shore J, Alshamrani M. 2018. A comprehensive analysis of anion-quadrupole interactions in protein structures. *Biochemistry* 57:1852–67
93. Bostick DL, Brooks CL 3rd. 2007. Selectivity in K⁺ channels is due to topological control of the permeant ion's coordinated state. *PNAS* 104:9260–65
94. Varma S, Sabo D, Rempe SB. 2008. K⁺/Na⁺ selectivity in K channels and valinomycin: over-coordination versus cavity-size constraints. *J. Mol. Biol.* 376:13–22

95. Fernandez R, Berro J. 2016. Use of a fluoride channel as a new selection marker for fission yeast plasmids and application to fast genome editing with CRISPR/Cas9. *Yeast* 33:549–57
96. Lellouche J, Friedman A, Gedanken A, Banin E. 2012. Antibacterial and antibiofilm properties of yttrium fluoride nanoparticles. *Int. J. Nanomed.* 7:5611–24
97. Li S, Breaker RR. 2012. Fluoride enhances the activity of fungicides that destabilize cell membranes. *Bioorg. Med. Chem. Lett.* 22:3317–22
98. Nelson JW, Zhou Z, Breaker RR. 2014. Gramicidin D enhances the antibacterial activity of fluoride. *Bioorg. Med. Chem. Lett.* 24:2969–71
99. Sherlock ME, Breaker RR. 2020. Former orphan riboswitches reveal unexplored areas of bacterial metabolism, signaling, and gene control processes. *RNA* 26:675–93
100. Zhao B, Guffy SL, Williams B, Zhang Q. 2017. An excited state underlies gene regulation of a transcriptional riboswitch. *Nat. Chem. Biol.* 13:968–74
101. Ren A, Rajashankar KR, Patel DJ. 2012. Fluoride ion encapsulation by Mg^{2+} ions and phosphates in a fluoride riboswitch. *Nature* 486:85–89
102. Jurcik A, Bednar D, Byska J, Marques SM, Furmanova K, et al. 2018. CAVER Analyst 2.0: analysis and visualization of channels and tunnels in protein structures and molecular dynamics trajectories. *Bioinformatics* 34:3586–88